Arabian Journal of Chemistry (2023) **16**, 104397

King Saud University

Arabian Journal of Chemistry

www.ksu.edu.sa
www.sciencedirect.com

ORIGINAL ARTICLE

3D hierarchical structure collaborating with 2D/2D interface interaction in $BiVO_4$/ZnCr-LDH heterojunction with superior visible-light photocatalytic removal efficiency for tetracycline hydrochloride

Ruofan Yang [a,b], Baiping Liang [a], Shizheng Zheng [a,*], Changyuan Hu [a,*], Yajuan Xu [c], Yanting Ma [a], Yangyang Bai [a], Kejie Dai [a], Yan Tang [a], Cuiqing Zhang [d], Miao Chang [a]

[a] *Jiangxi Key Laboratory of Surface Engineering (School of Materials and Mechanical & Electrical Engineering), Jiangxi Science and Technology Normal University, Nanchang 330013, PR China*
[b] *Key Laboratory of Bio-based Material Science and Technology (Ministry of Education), Northeast Forestry University, 26 Hexing Road, Harbin 150040, PR China*
[c] *Institute of Foreign Languages, Jiangxi Science and Technology Normal University, Nanchang 330013, PR China*
[d] *School of Pharmacy, Jiangxi Science and Technology Normal University, Nanchang 330013, PR China*

Received 27 June 2022; accepted 5 November 2022
Available online 11 November 2022

KEYWORDS

$BiVO_4$;
ZnCr-LDH;
Hierarchical structure;
Type II heterojunction;
Photocatalysis

Abstract Fabrication of heterojunction with specialized geometry shape could improve the photodegradation efficiency of catalysts more efficiently based on the synergistic effect of components. Herein, the $BiVO_4$/ZnCr-LDH type-II heterojunction was successfully synthesized by the growth of two-dimensional (2D) ZnCr-LDH on 2D $BiVO_4$, forming a unique three-dimensional (3D) hierarchical structure. The 3D hierarchical $BiVO_4$/ZnCr-LDH type-II heterojunction with intimate 2D/2D heterointerfaces enlarges the interfacial contact areas and shortens the transfer distance of carriers simultaneously, which could promote the separation and transfer of photoinduced carriers and prolong the lifetime of carriers. Additionally, the 3D structure could enhance the photon utilization efficiency caused by the multiple reflections of incident light, and provide more active

* Corresponding authors.
E-mail addresses: zhengsz1990@163.com (S. Zheng), hcy6257@163.com (C. Hu).
Peer review under responsibility of King Saud University.

Production and hosting by Elsevier

https://doi.org/10.1016/j.arabjc.2022.104397
1878-5352 © 2022 The Author(s). Published by Elsevier B.V. on behalf of King Saud University.
This is an open access article under the CC BY-NC-ND license (http://creativecommons.org/licenses/by-nc-nd/4.0/).

sites to promote the adsorption of pollutants. Therefore, the visible light catalytic performance of the optimal heterostructure for the removal of tetracycline hydrochloride is 3.47 times and 22.43 times higher than that of $BiVO_4$ and ZnCr-LDH, respectively. Superoxide radical ($\cdot O_2^-$) is confirmed as the primary active species, whereas hole (h^+) is the secondary active species in the photodegradation process. This work provides a facile strategy to enhance the visible light catalytic behavior of $BiVO_4$ through the fabrication of 3D hierarchical architecture heterojunction for the removal of organic pollutant.

© 2022 The Author(s). Published by Elsevier B.V. on behalf of King Saud University. This is an open access article under the CC BY-NC-ND license (http://creativecommons.org/licenses/by-nc-nd/4.0/).

1. Introduction

Semiconductor photocatalysts can utilize the inexhaustible and clean sunlight to effectively degrade contamination, which can alleviate serious resource and worldwide environmental issues (Li et al., 2019a; Wang et al., 2022; Wu et al., 2022; Yang et al., 2022a). Up to now, various 2D(two-dimensional) bismuth-based photocatalysts, including Bi_2O_2S (Xing et al., 2019), $Bi_2O_2CO_3$ (Tan et al., 2021), BiOBr (Yang et al., 2022b) and Bi_2WO_6 (Li et al., 2022b), have been developed as candidates for mitigating the deterioration of environments. Among the various 2D nanosheets, monoclinic $BiVO_4$ with a 2D structure has attracted widespread attention for its narrow band gap (~2.4 eV), adjustable structure and high visible light absorption property (Liu et al., 2020a; Ni et al., 2018; Shen et al., 2020). Unfortunately, though tremendous efforts have been made by scientists for $BiVO_4$ catalysts, the insufficient separation of photo-generated carriers and relatively low utilization of solar energy still preclude its potential application in the field of photodegradation (Lu et al., 2020; Zhou et al., 2019; Zhao et al., 2016). Therefore, it is highly desirable to promote the migration and separation of photoexcited carriers and extend the spectral response range for improving the photocatalytic performance of $BiVO_4$.

To address the above issues, many attempts, including defects engineering (Yao et al., 2019), dye-sensitized (Sun et al., 2015), fabrication of hierarchical structure (Yang et al., 2020), coupling with other semiconductors (Li et al., 2022c), etc., have been implemented to enhance the photodegradation efficiency of $BiVO_4$ nanosheets. The construction of the $BiVO_4$-based junction with matching bandgap energy like type II (Li et al., 2021b), P-N (Ma et al., 2022) and Z-scheme (Dong et al., 2018) heterojunction, is an impactful tactic to improve the separation efficiency of photoinduced carriers and sunlight absorption capability. Although numerous $BiVO_4$-based heterojunctions have been investigated to accelerate the interfacial photoinduced carriers' separation and migration, the morphology design of junctions is often neglected (Li et al., 2018). In fact, the design of the geometry such as core–shell structure (Li et al., 2019b), hollow sphere structure (Li et al., 2022a), 2D/2D structure (Le et al., 2019), 3D hierarchical architecture (Ren et al., 2021) etc., has a positive and synergistic effect on enhancing the catalytic performance of photocatalysts. In comparison with the 0D (zero-dimensional), 1D (one-dimensional) and 2D structures, the unique 3D hierarchical structure collaborating with the close 2D/2D heterostructure interface can greatly shorten the diffusion pathway of carriers, which is very helpful for improving the charge carriers' separation efficiency (Yang et al., 2020; Kong et al., 2021; Ren et al., 2021). In addition, due to the multi-reflections for incident light, almost all of incident photons can be harvested by the hierarchical structured material, leading to the enhanced spectral utilization efficiency (Yang et al., 2022b). Furthermore, the 3D hierarchical structures could also raise the specific surface area to expose more active sites, thus enhancing the adsorption capability for reactants and speeding up the redox reactions (Shen et al., 2020). In light of these views, a large number of heterojunctions with 3D hierarchical structure have been successfully designed and synthesized, such as NiAl-LDH (Layered double hydroxide)/Ti_3C_2 (Shi et al., 2021), Bi_2O_3/Bi_2WO_6/MgAl-CLDH (Bing et al., 2018), $InVO_4/Ti_3C_2T_x$ (Li et al., 2021a), Ag@AgBr/ZnCr-LDH (Sahoo et al., 2018), WO_3@BiOBr (Ling et al., 2020), CuS@$ZnIn_2S_4$ (Fan et al., 2022). For $BiVO_4$, the 3D hierarchical structured hybrids also demonstrate superior photodegradation performance toward pollutants. For instance, a novel 3D/2D $BiVO_4$@PPy/g-C_3N_4 Z-scheme heterojunction was successfully fabricated via the one-step hydrothermal method, which displayed excellent photodegradation efficiency and stability toward tetracycline hydrochloride (TC) under the visible light irradiation, due to the rapid separation of photogenerated carriers via unique coupling heterointerface (Yan et al., 2021). In addition, Sun et al. combined an in-situ deposition method with ultraviolet light irradiation to prepare 3D plasmonic Ag/Ag_2S/$BiVO_4$ p-n heterojunction, in which the Ag/Ag_2S was coated onto the surface of $BiVO_4$ sheets, with much higher photocatalytic performance for the oxidation of oxytetracycline hydrochloride and reduction of Cr^{6+} than $BiVO_4$ under visible light irradiation (Wei et al., 2018). These works strongly confirm that the fabrication of 3D hierarchical heterojunction constructed by 2D sheets is an efficient tactic to improve the photodegradation efficiency of photocatalysts.

LDH is expressed as $[M^{2+}_{1-x}M^{3+}_x\ (OH)_2]\ (A^{n-})^{x/n}\cdot mH_2O$, where M^{2+}, M^{3+}, A^{n-} represents a divalent metal cation, trivalent metal cation and interlayer anion, respectively, and × is the molar ratio of trivalent metal ion to total metal ion (Cui et al., 2021). Thanks to its unique 2D brucite-like layered structure, high surface area, tunable metal cation structure, and interlayer anion exchange capacity; various LDH catalysts could adsorb pollutant molecules from solutions, enriching the pollutant molecules to the LDH surface, which could undoubtedly promote the catalytic reaction (Fu et al., 2016; Lan et al., 2014). Furthermore, LDH can harvest visible light through interelectronic excitation such as intermetallic charge transfer (MMCT) and ligand-to-metal charge transfer (LMCT) (Liu et al., 2017). Importantly, LDH nanosheets could interact with other catalysts to self-assemble into 3D hierarchical composites with unique architectures, due to their inherent positive charge and the abundant ionic surface − OH group (Shi et al., 2021; Sun et al., 2014). Among the various LDH catalysts, ZnCr-LDH has been found to be effective in the field of photocatalysis due to its appropriate redox potential and superior light-harvesting capability (Zheng et al., 2021). For example, a novel Cu_2O@ZnCr-LDH core–shell heterojunction has displayed the excellent photocatalytic H_2/O_2 production efficiency under the visible light irradiation (Wang et al., 2017). Therefore, ZnCr-LDH may be the suitable candidate in collaboration with $BiVO_4$ to construct a 3D hierarchical heterostructure.

Herein, a novel two-step hydrothermal approach was employed to fabricate 3D hierarchical $BiVO_4$/ZnCr-LDH type II heterostructure by coupling 2D ZnCr-LDH nanosheets and 2D $BiVO_4$ nanosheets with controllable constituent ratio. The various characterizations techniques were used to determine the morphology, crystallinity and optical property of $BiVO_4$/ZnCr-LDH type II junctions. The catalytic activity of $BiVO_4$/ZnCr-LDH hybrid was evaluated by the photodegradation of TC under visible-light irradiation. The 3D hierarchical $BiVO_4$/ZnCr-LDH junctions exhibit much higher photodegradation efficiency than bare $BiVO_4$ and ZnCr-LDH nanosheets. The results of the trapping experiment and the electron spin resonance (ESR) indicate that $\bullet O_2^-$ is the primary active species,

whereas h^+ is the secondary active species in the catalytic system. Additionally, a probable catalytic mechanism for the removal of TC over 3D hierarchical $BiVO_4$/ZnCr-LDH heterostructure is posed according to the various characterization results.

2. Experimental

2.1. Materials

Bismuth nitrate pentahydrate ($Bi(NO_3)_3{\bullet}5H_2O$), zinc nitrate hexahydrate ($Zn(NO_3)_2{\bullet}6H_2O$), chromium nitrate nonahydrate ($Cr(NO_3)_3{\bullet}9H_2O$), ammonium metavanadate (NH_4VO_3), sodium hydroxide (NaOH), sodium carbonate (Na_2CO_3), sodium oxalate ($Na_2C_2O_4$), benzoquinone (BQ), isopropanol (IPA), sodium dodecyl benzene sulfonate ($C_{18}H_{29}NaO_3S$) and TC were supplied by Sinopharm Chemical Reagent Co., ltd. All reagents were of analytical grade and were not further purified.

2.2. Synthesis of the photocatalysts

$BiVO_4$ was synthesized by the hydrothermal method in deionized (DI) water according to previously reported work (Sun et al., 2019). The 3D hierarchical $BiVO_4$/ZnCr-LDH type II heterojunction was also fabricated by the hydrothermal method. Briefly, 7.68 g NaOH and 6.36 g Na_2CO_3 powers were dispersed in 100 mL DI water, and electromagnetically stirred until transparent, which was later denoted as solution A for later use. Then, a certain amount of $Zn(NO_3)_2{\bullet}6H_2O$, $Cr(NO_3)_3{\bullet}9H_2O$ (the molar ratio of $Zn(NO_3)_2{\bullet}6H_2O$/$Cr(NO_3)_3{\bullet}9H_2O$ is fixed at 2) and 1 mmol $BiVO_4$ powders were dispersed in 30 mL DI water, named as the solution B. Subsequently, the mixed solution A was gradually added into the solution B for keeping the constant pH of the mixture at 7. The above resultant solution was filled into a 50 mL sealed autoclave, and heated at 120 °C for 24 h. After collected by centrifugation (6000 rpm), the catalysts were dried overnight. The samples are marked as x-B-ZCL, where × represents the molar ratio of $BiVO_4$ to Zn $(NO_3)_2{\bullet}6H_2O$. Pure ZnCr-LDH was also prepared without the addition of $BiVO_4$ by the above approach.

2.3. Sample characterizations

The crystalline structure of catalysts was probed by X-ray power diffraction (XRD) (Japan, XRD6100), which used Cu Kα radiation. The scanning electron microscope (SEM) (Zeiss, Sigma) and the transmission electron microscope (TEM) (FEIG2) images were obtained to study the morphology of the catalysts. The UV–vis optical absorption was conducted with a UV–vis spectrophotometer (UV-2550, Shimadzu, Japan). The chemical states of catalysts were investigated using the X-ray photoelectron spectroscopy (XPS) (Thermo Scientific K-Alpha$^+$). The ESR data was recorded on a Bruker A200 spectrometer (Germany). The Brunauer-Emmett-Teller (S_{BET}) specific surface areas were evaluated by nitrogen (N_2) adsorption–desorption (Quantachrome ASIQM000-200–6). The total organic carbon content (TOC) removal efficiency of TC was analyzed on a TOC-2000 (Metash, China) analyzer. Photoluminescence (PL) spectroscopy measurements were identified by F-4600. The transient photocurrent response, the Mott-Schottky (M−S) measurements and the electrochemical impedance spectroscopy (EIS) were characterized by electrochemical workstation (CHI-660E).

2.4. Catalytic activity measurements

To test the catalytic efficiency of catalysts under visible-light irradiation, TC was selected as the refractory organic. 30 mg catalysts were diffused into a 50 mL TC (40 mg/L) suspension. A 500 W xenon lamp was used as the visible light source, equipped with a 420 nm cut-off filter. The mixture was ultrasonicated for a few minutes and vigorously stirred in the dark for 0.5 h to attain the adsorption–desorption equilibrium. Then the suspension was irradiated with visible light. At certain time intervals, aliquots (4 mL) of the mixture were intermittently sampled and filtered to eliminate the catalyst precipitates. Lastly, the filtrate was analyzed using UV–vis spectrophotometer. The trapping experiments were conducted by adding scavengers to TC solution, including IPA, BQ, and $Na_2C_2O_4$. The other experiment procedure was similar to that of the catalytic degradation experiment.

3. Results and discussion

3.1. Structure characterization

The overall synthetic route of the 3D hierarchical $BiVO_4$/ZnCr-LDH type II heterojunction is shown in Scheme 1. The phase and crystalline structure of the catalysts were characterized by the XRD patterns. In Fig. 1, the diffraction peaks located at 2θ = 15.1°, 18.7°, 28.8°, 34.5°, 39.5°, and 42.3° can be well matched with the (0 2 0), (1 1 0), (−1 2 1), (2 0 0), (−1 4 1) and (1 5 0) planes of monoclinic $BiVO_4$ phase (JCPDS card No. 14–0688), respectively(Sun et al., 2019; Tang et al., 2014). As-prepared ZnCr-LDH (JCPDS card No.51–1525) has obvious diffraction peaks at 11.7°, 23.5°, 34.9°, 39.5°, 47.0°, 60.7°, and 62.1° could be assigned to the crystal planes of (0 0 3), (0 0 6), (0 1 2), (0 1 5), (0 1 8), (1 1 0) and (1 1 3), respectively (Wang et al., 2017; Sun et al., 2014). For $BiVO_4$/ZnCr-LDH heterojunction, when the content of ZnCr-LDH is relatively low, the peaks of ZnCr-LDH can hardly be seen, such as 3-B-ZCL. When the molar ratio of $BiVO_4$ to Zn $(NO_3)_2{\bullet}6H_2O$ is further decreased to 1, the characteristic peaks of both $BiVO_4$ and ZnCr-LDH could be detected. The peak intensities of the ZnCr-LDH at 11.7° and 23.5° gradually heighten with the increase of ZnCr-LDH content, while that of $BiVO_4$ drops step by step. The reason may be that ZnCr-LDH coated onto the surface of $BiVO_4$ nanosheets shield partially the diffraction peaks of $BiVO_4$, which will be confirmed by the following SEM and TEM images.

The micromorphology of $BiVO_4$, ZnCr-LDH and 0.5-B-ZCL heterojunction was observed by SEM and EDS mapping images. As depicted in Fig. 2a, the 2D irregular ZnCr-LDH nanosheets with a lateral size of 30–50 nm stack each other, which effortlessly gather in cohesive force, consistent with previous literature (Sohail et al., 2019; Sahoo et al., 2019). Fig. 2b shows that pure $BiVO_4$ is also an irregular 2D flake-like structure with a smooth crystal surface, which provides a favorable platform for the loading of ZnCr-LDH onto the surface (Lu et al., 2020). For B-ZCL heterojunction, taking 0.5-B-ZCL as an example, unlike pure $BiVO_4$ with a smooth surface, some

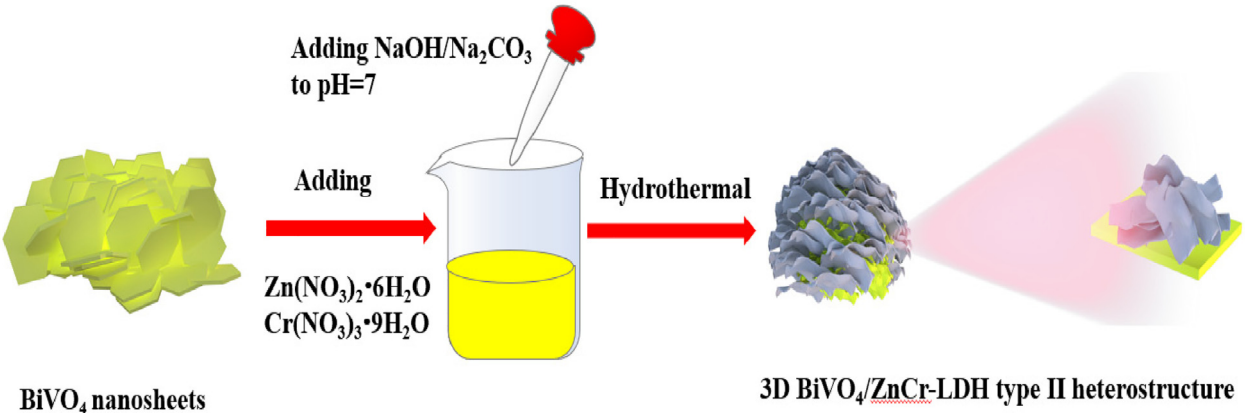

Scheme 1 Schematic illumination for the preparation of 3D $BiVO_4$/ZnCr-LDH type II heterojunction.

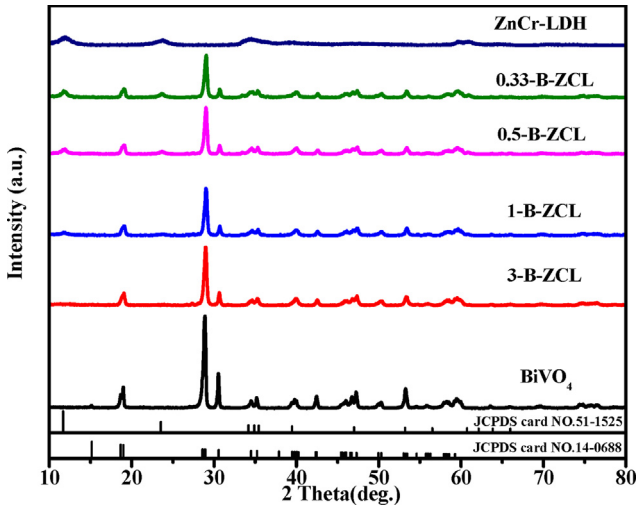

Fig. 1 XRD patterns of ZnCr-LDH, $BiVO_4$ and a series of B-ZCL heterojunctions.

stacked 2D ultrathin ZnCr-LDH nanosheets were loaded in situ on the surface of 2D $BiVO_4$ after hydrothermal reaction, forming a 3D hierarchical structured B-ZCL heterojunction (Fig. 2c). This unique structure could expose more active sites and increase the contact area of the catalysts, contributing to improve the separation efficiency of photo-induced carriers, which is conducive to improve the photocatalytic performance (Liu et al., 2020b). Furthermore, as displayed in Fig. 2d–i, to investigate the surface elemental composition, the EDS mapping spectra imply the coexistence of Zn, Cr, O, C, Bi and V elements on the 0.5-B-ZCL heterojunction. Additionally, compared to Bi and V elements, Zn, Cr, O and C elements are more densely distributed, which also confirms that ZnCr-LDH has been tightly well integrated onto the $BiVO_4$ surface with close interfacial contact. As further confirmed by the TEM images, a large number of accumulated 2D ZnCr-LDH nanosheets with a lateral size of 30 $\sim$ 50 nm is agglomerated together, while pure $BiVO_4$ is an irregular 2D flake-like structure with several hundred nanometers in length (Fig. 3a-b). As shown in Fig. 3c, taking 0.5-B-ZCL as an example, the close contact between 2D ZnCr-LDH nanosheets and 2D flake-shaped $BiVO_4$ is clearly observed, along with distinct heterogeneous interface and boundary contours, which is consistent with SEM results. The (−141) crystal planes of $BiVO_4$ with the interplanar spacings of 0.228 nm can be seen from the HRTEM image, while the interplanar spacing of LDH is unclear, possibly due to the lower crystallinity (Guo et al., 2019) (Fig. 3d). Therefore, it is rationally concluded that 3D hierarchical $BiVO_4$/ZnCr-LDH heterojunction with good contact interface has been successfully synthesized, which will promote the migration and separation efficiency of photo-induced carriers and extend the spectrum absorption range.

The XPS spectra were used to explore the surface composition and elemental chemical states of the $BiVO_4$, ZnCr-LDH and 0.5-B-ZCL heterojunction. Fig. 4a exhibits the coexistence of Bi, O, V, Zn, Cr, and C elements in 0.5-B-ZCL heterojunction, compared to pristine $BiVO_4$ and ZnCr-LDH. In Fig. 4b, the Bi $4f_{7/2}$ and Bi $4f_{5/2}$ of $BiVO_4$ assignments of Bi^{3+} could be fitted as characteristic double peaks with a binding energy of 158.9 eV and 164.2 eV. In Fig. 4c, the spectra of V 2p can be deconvoluted well into two peaks with binding energies of 516.4 and 523.9 eV, which are put down to the V $2p_{3/2}$ and V $2p_{1/2}$, respectively. Compared to $BiVO_4$, the binding energy of Bi 4f and V 2p in 0.5-B-ZCL heterojunction exhibits a slight shift to lower energy, indicating the electrons are migrated from ZnCr-LDH to $BiVO_4$ surface, owing to a powerful interface interaction between $BiVO_4$ and ZnCr-LDH (Wei et al., 2018; Yan et al., 2021). For Zn and Cr elements, the binding energies of Zn $2p_{3/2}$ (Zn $2p_{1/2}$) and Cr $2p_{3/2}$ (Cr $2p_{1/2}$) are positively shifted by 0.1 eV in relation to the original ZnCr-LDH (Fig. 4d-e). Meanwhile, two binding energy values of 284.8 and 288.8 eV are observed for C 1s in ZnCr-LDH, which indicates the presence of reference carbon and the intercalated CO_3^{2-} anions in the layered structure of ZnCr-LDH (Tian et al., 2012; Sun et al., 2014). Similarly, compared to ZnCr-LDH, the C 1s binding energy in 0.5-B-ZCL heterojunction is slightly moved to higher energy. From the results of XPS, the surface modification of $BiVO_4$ by ZnCr-LDH induces a slight shift of both Bi 4f and V 2p peaks toward lower energy, while the peaks of Zn 2p, Cr 2p and C 1s move in the opposite direction, which demonstrates the electrons are transferred from ZnCr-LDH to $BiVO_4$ due to a strong interfacial interaction.

The specific surface areas (S_{BET}) and pore volume values of ZnCr-LDH, $BiVO_4$ and B-ZCL heterojunctions were analyzed by N_2 adsorption–desorption experiment. As shown in

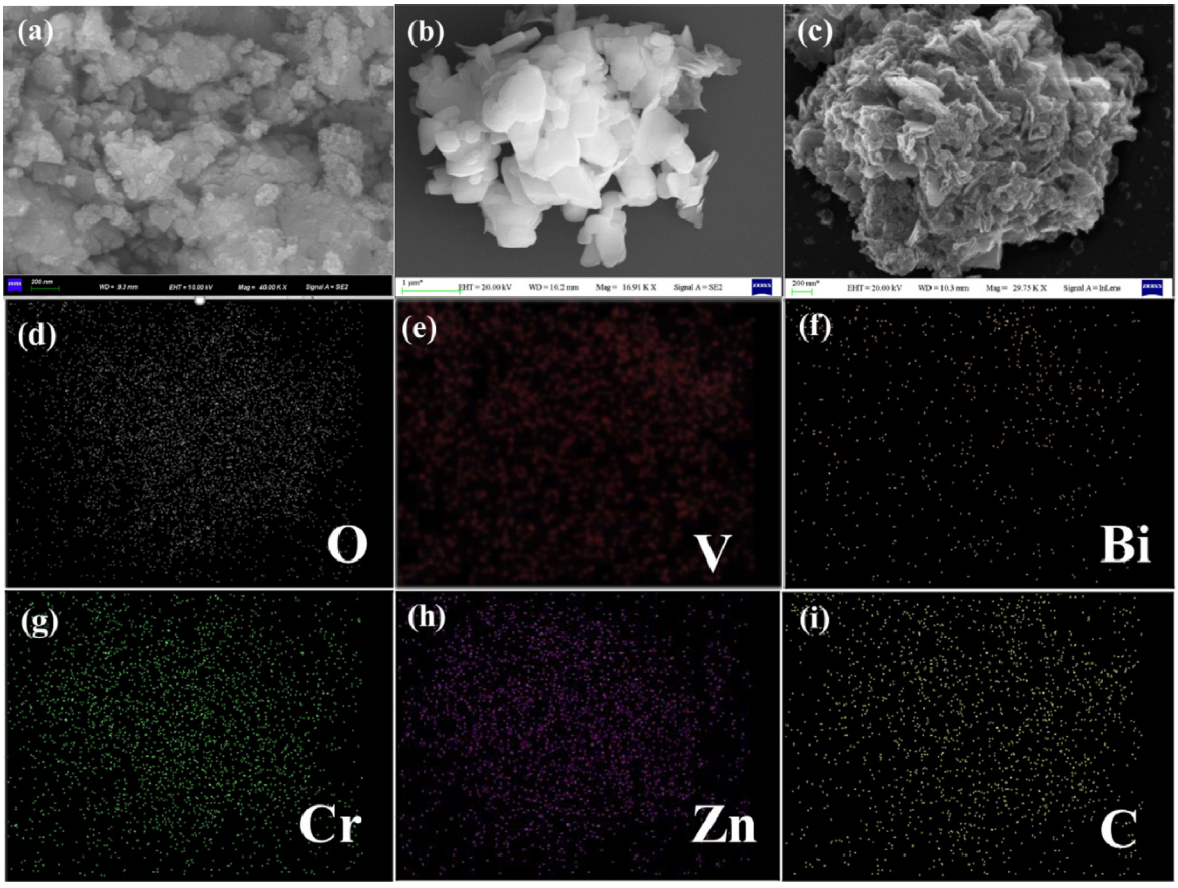

Fig. 2 SEM images of ZnCr-LDH (a), $BiVO_4$ (b), 0.5-B-ZCL (c) and EDS-mapping images (d–i).

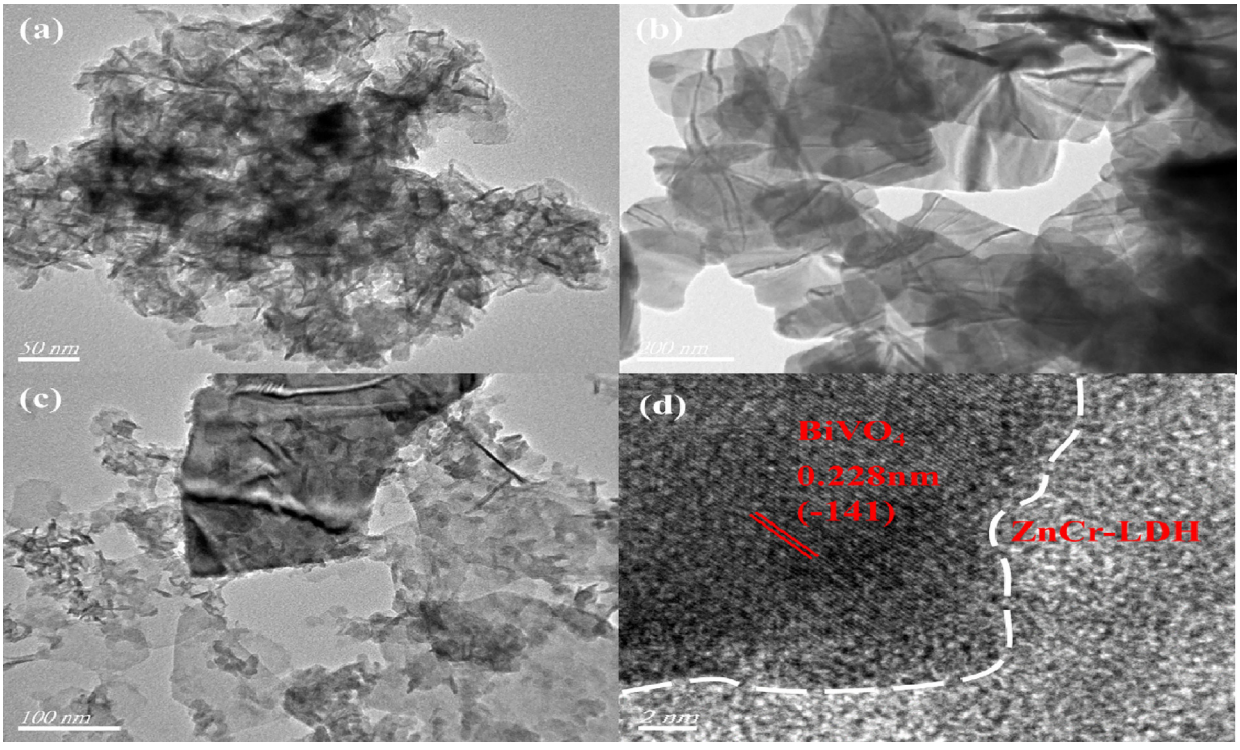

Fig. 3 TEM images of ZnCr-LDH (a), $BiVO_4$ (b), 0.5-B-ZCL (c) and HRTEM images of 0.5-B-ZCL heterojunction (d).

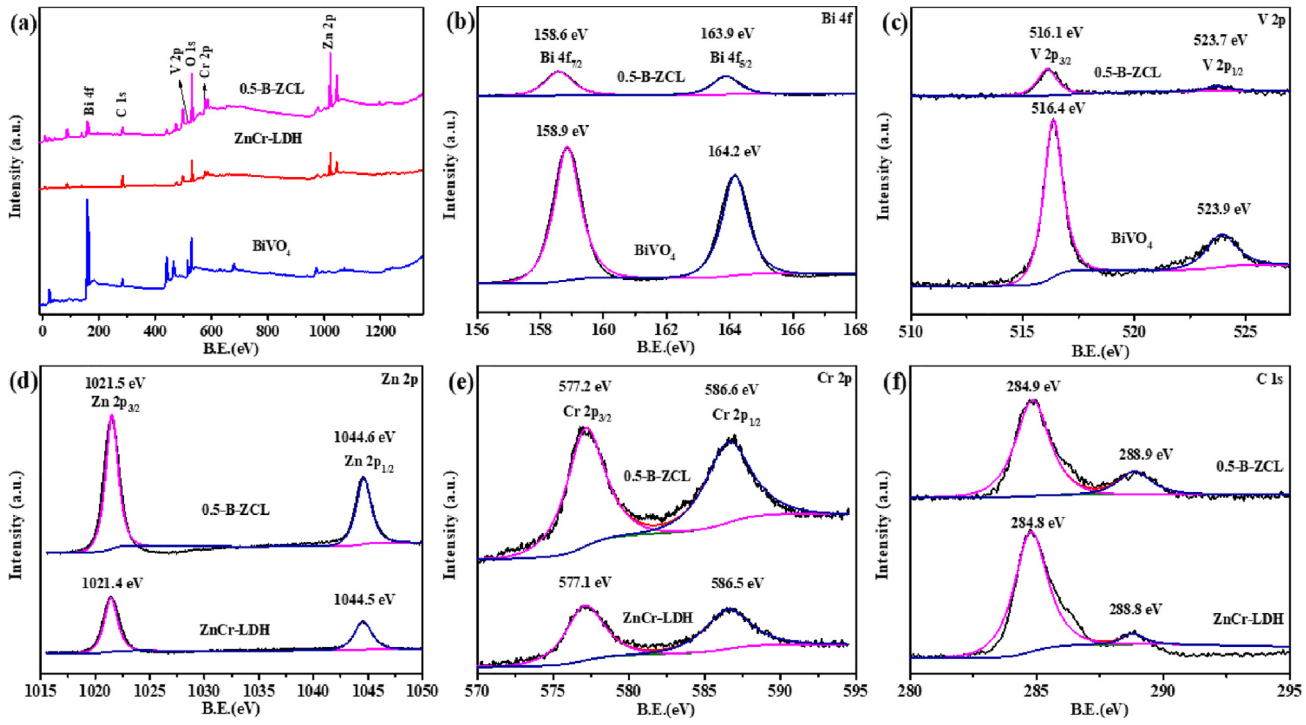

Fig. 4 XPS spectra of ZnCr-LDH, $BiVO_4$ and 0.5-B-ZCL heterojunction: survey (a), Bi 4f (b), V 2p (c), Zn 2p (d), Cr 2p (e), C 1s (f).

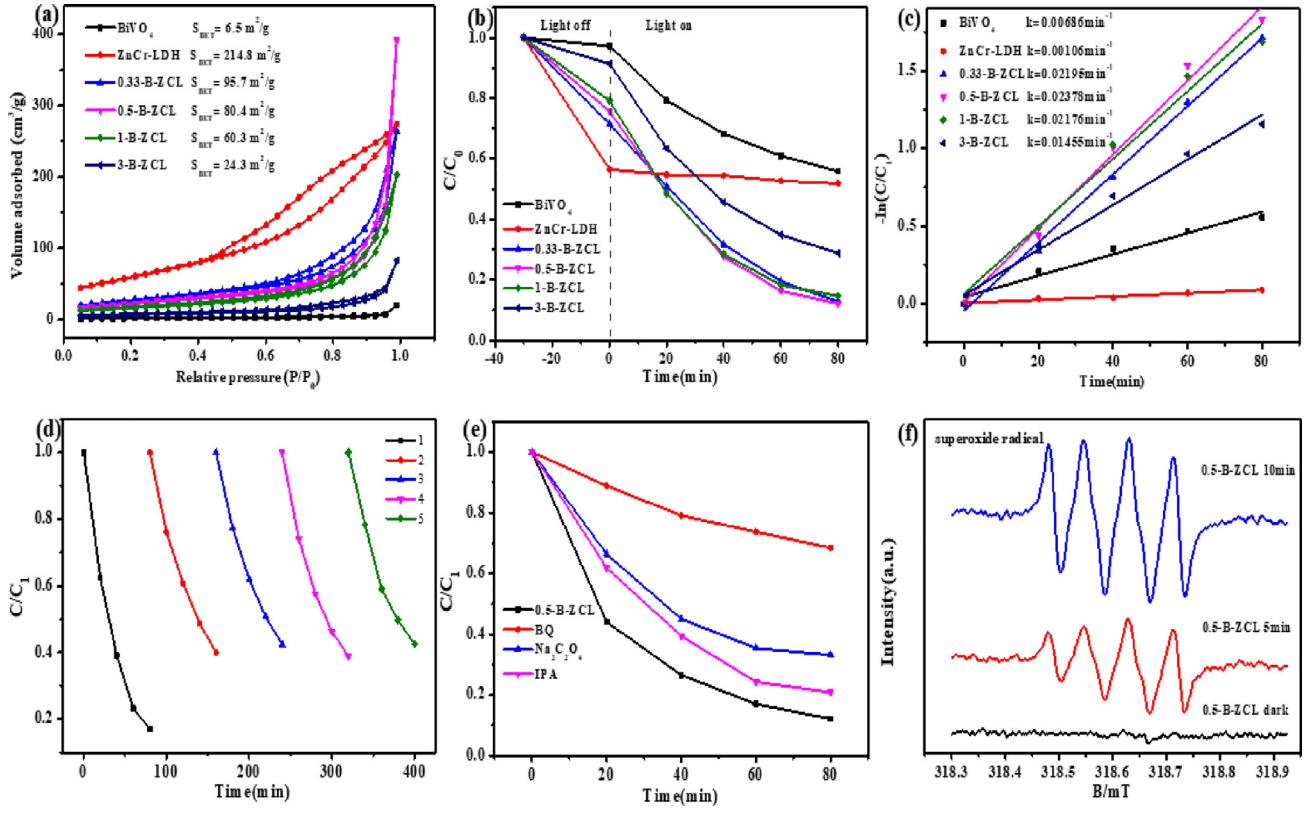

Fig. 5 N_2 adsorption–desorption isotherms of ZnCr-LDH, $BiVO_4$ and a series of B-ZCL heterojunctions (a); Photocatalytic degradation activity (b) and kinetic curve of degradation for TC (c) in the presence of ZnCr-LDH, $BiVO_4$ and a series of B-ZCL heterojunctions; Cycling experiments (d), quenching experiment (e), and ESR spectra (f) for TC degradation over 0.5-B-ZCL heterojunction under visible-light irradiation.

Fig. 5a, $BiVO_4$ is a type-II adsorption isotherm, indicating a non-porous structure (Yan et al., 2021), consistent with its morphology observed from SEM images. Conversely, ZnCr-LDH and B-ZCL heterojunctions can be assigned as a type-IV adsorption isotherm with H_3 hysteresis loop, implying the presence of mesopore generated from the aggregated nanosheets (Liu et al., 2017). As can be seen from Table 1, the S_{BET} of ZnCr-LDH and $BiVO_4$ are 214.8 m^2/g and 6.5 m^2/g, while their pore volume values are 0.42 cm^3/g and 0.03 cm^3/g, respectively. Compared to $BiVO_4$, the S_{BET} and pore volume values of B-ZCL heterojunction structures are increased. On the whole, with the increase of ZnCr-LDH content, the S_{BET} and pore volume values of B-ZCL heterojunctions rise gradually. In detail, the S_{BET} of 3-B-ZCL, 1-B-ZCL and 0.5-B-ZCL are 24.3 m^2/g, 60.3 m^2/g and 80.4 m^2/g, respectively. The pore volume values of 3-B-ZCL, 1-B-ZCL and 0.5-B-ZCL are 0.13 cm^3/g, 0.32 cm^3/g and 0.60 cm^3/g, respectively. Though the S_{BET} of 0.33-B-ZCL is further raised to 95.7 m^2/g, its pore volume is decreased to 0.41 cm^3/g. Clearly, 0.5-B-ZCL with a loosely layer-by-layer stacking has a relatively larger S_{BET} and the maximum pore volume values. Generally speaking, the higher S_{BET} and pore volume could provide more active sites and channels, thus improving the catalytic efficiency (Sahoo et al., 2019).

3.2. Photocatalytic performance of catalysts

To reflect the adsorption capacity of catalysts in the absence of light, the photocatalytic degradation activity including the adsorption of pollutants in the aqueous solution under dark conditions is shown in Fig. 5b. The removal efficiency is defined as C/C_0, in which C and C_0 stand for the remnants and initial concentration of TC, respectively. Before the photocatalytic degradation, the solution including TC and catalysts is stirred in the dark for 30 min to reach the adsorption equilibrium. The $BiVO_4$ (2.7 %) has a much weaker adsorption performance in comparison with pristine ZnCr-LDH (43.5 %). Nevertheless, the B-ZCL heterojunctions exhibit gradually improved adsorption performance with the increase of ZnCr-LDH content. For example, the adsorption efficiency of TC for the optimal 0.5-B-ZCL sample is up to 24.3 % in the same time range. The above results imply that the construction of B-ZCL junction has a positive effect on the adsorption performance, compared with the $BiVO_4$ alone.

The total removal rate of ZnCr-LDH and $BiVO_4$ for TC is only as low as 48.2 % and 44.1 % after visible light photocatalytic reaction for 80 min, respectively. Obviously, the B-ZCL heterojunctions show superior removal efficiency to the single component. When a small amount of $BiVO_4$ is recombined with ZnCr-LDH, the construction of 0.33-B-ZCL junction could significantly enhance its visible light catalytic efficiency. With the increase of ZnCr-LDH content, the photodegradation efficiency of TC for the 0.5-B-ZCL heterojunction reaches the optimum (87.9 %) under the same condition. Continuing to increase the content of LDH, the photodegradation performance of B-ZCL heterojunction starts to decline. To directly explore the catalytic removal efficiency, degradation kinetics of TC over all samples are simulated by $\ln(C_0/C) = kt$ (Yang et al., 2022a). In Fig. 5c, the rate constant of $BiVO_4$, ZnCr-LDH, 0.33-B-ZCL, 0.5-B-ZCL, 1-B-ZCL and 3-B-ZCL is fitted as 0.00686 min^{-1}, 0.00106 min^{-1}, 0.02195 min^{-1}, 0.02378 min^{-1}, 0.02176 min^{-1} and 0.01455 min^{-1}, respectively. The rate constant for the optimal 0.5-B-ZCL heterojunction is 3.47 times and 22.43 times higher than that of $BiVO_4$ and ZnCr-LDH for the TC antibiotic. The superior catalytic degradation efficiency of B-ZCL heterojunction should relate to its unique 3D hierarchical heterostructure, which could not only facilitate the separation of photo-triggered carriers upon visible light irradiation, but also increase the utilization of incident photons as well as, enlarge the specific surface areas and improve the adsorption capability for TC. Furthermore, our $BiVO_4$/ZnCr-LDH heterostructure exhibits much higher photocatalytic degradation activity for TC compared with related $BiVO_4$-based photocatalysts (Table 2).

The cycling performance is important for the practical application of the photocatalyst. Consequently, the used 0.5-B-ZCL heterojunction is collected through a series of procedures including filtering, washing, and drying to demonstrate its photostability. As shown in Fig. 5d, although the photodegradation efficiency dramatically decreases from 82.9 % to 60.0 % under visible light illumination after the second cycle, the degradation efficiency of the 0.5-B-ZCL heterojunction remains about 60.0 % in the following cycles. The XRD and SEM were applied to characterize the crystalline structure and morphology of 0.5-B-ZCL after the recycling experiments. As displayed in Fig. S1a, the peak intensities of the $BiVO_4$ in the 0.5-B-ZCL-after sample gradually heighten, compared with the 0.5-B-ZCL-before sample, indicating that the part of ZnCr-LDH may be slightly peeled off during the cycle runs. Nevertheless, it can be obviously observed that the morphology of the 0.5-B-ZCL-after sample remains unchanged after five cycling experiments (Fig. S1b). These results demonstrate that the $BiVO_4$/ZnCr-LDH heterojunction has relative stability to some extent.

To further discuss the generation of reactive oxygen species, the active species for the photodegradation of TC over 0.5-B-ZCL heterojunction were explored by a radical quenching experiment. As shown in Fig. 5e, $Na_2C_2O_4$, BQ and IPA were applied to probe the active species like h^+, $\bullet O_2^-$, and •OH, respectively (Li et al., 2021b). When a certain amount of BQ is added to the photocatalytic system, the catalytic activity of 0.5-B-ZCL heterojunction is completely suppressed, indicating that $^{\bullet}O_2^-$ is the dominant active species. By introducing $Na_2C_2O_4$ into the catalytic reaction, the degradation activity for TC

Table 1 Summary of the textural properties of samples.

Samples	ZnCr-LDH	$BiVO_4$	3-B-ZCL	1-B-ZCL	0.5-B-ZCL	0.33-B-ZCL
S_{BET} (m^2/g)	214.8	6.5	27.3	60.3	80.4	95.7
Pore volume(cm^3/g)	0.42	0.03	0.13	0.32	0.60	0.41

Table 2 A comparison of photocatalytic degradation performance for TC over $BiVO_4$/ZnCr-LDH junction with related $BiVO_4$-based photocatalysts.

Catalyst	Dosage (mg)	Concentration of TC (mg/L)	Source	Reaction time (min)	Removal percentage (%)	Ref.
$BiVO_4$/ZnCr-LDH	30	40	Visible light	80	87.9	This work
$BiVO_4$/Nitrogen-doped carbon quantum dots	50	5	Visible light	150	93.5	Liu et al. (2020a)
$BiVO_4$/g-C_3N_4 quantum dots	30	20	Visible light	60	73.8	Li et al. (2019a)
AgI/$ZnIn_2S_4$/$BiVO_4$	30	20	Visible light	120	91.4	Wang et al. (2022)
$In_{2.77}S_4$/$BiVO_4$	50	10	Visible light	90	89.9	Wu et al. (2022)
$BiVO_4$@PPy/g-C_3N_4	30	30	Visible light	120	90	Yan et al. (2021)

is decreased to 66.8 %, suggesting h^+ is the secondary active species. After adding IPA into the system, the catalytic activity of 0.5-B-ZCL is only slightly decreased, which means that •OH hardly works during the photocatalytic reaction. The above experiment results suggest that $\cdot O_2^-$ is the dominant active species, whereas h^+ is another active species in the catalytic system. Besides, the ESR method was further measured to test the active species in the catalytic process of TC. Specifically, $\cdot O_2^-$ generated from the reduction of O_2 by electrons, which can be investigated by probing the 5, 5-dimethyl-1-pyrroline (DMPO)-$\cdot O_2^-$ in a methanol medium. For 0.5-B-ZCL (Fig. 5f), no signal peaks are observed in the dark. However, the peaks corresponding to DMPO-$\cdot O_2^-$ could be observed under visible light illumination. Therefore, $\cdot O_2^-$ and h^+ are the major active species during the catalytic reaction.

3.3. Optical absorption Property, band structure and charge separation

The UV–vis diffuse absorption spectrogram was utilized to characterize the light absorption performance of ZnCr-LDH, $BiVO_4$ and B-ZCL heterojunction. In Fig. 6a, the optical absorption edge of $BiVO_4$ is about 514 nm, while the two strong characteristic peaks of ZnCr-LDH at around 410 and 570 nm can be seen, corresponding to LMCT transition from O 2p orbital to Cr^{3+} 3d orbital and MMCT spectra attributed to d-d transition from Cr 3dt2g to Cr 3 deg orbitals, respectively (Sahoo et al., 2018; Sahoo et al., 2019). Meanwhile, a strong absorption peaks ranging from 230 to 320 nm is also observed for ZnCr-LDH, which is assigned as the LMCT transition between Cr 3dt2g and Zn 4 s orbitals (Liu et al., 2018). Compared to $BiVO_4$, the optical absorption edge of B-ZCL heterojunction exhibits an apparent red shift, and a raised tail appears obviously in the range of 500–600 nm with the increased content of ZnCr-LDH. Furthermore, the band gap (Eg) values are calculated by Kubelka-Munk equation: $\alpha h\nu^{1/n} = A(h\nu - E_g)$, where α, $h\nu$, A is absorption coefficient, photon energy, a constant, respectively, and n is determined by semiconductor intrinsic property (Yang et al., 2022b). According to previous reports, ZnCr-LDH and $BiVO_4$ are all direct bandgap semiconductors, so n is equal to 2 (Wang et al., 2017; Li et al., 2021b). In Fig. 6b-c, the Eg of ZnCr-LDH and $BiVO_4$ is calculated approximately to be 2.50 eV and 2.41 eV, respectively. To further verify the band structure of ZnCr-LDH and $BiVO_4$, the M−S test was performed to investigate the flat band potential (E_{fb}). The E_{fb} of ZnCr-LDH and $BiVO_4$ are −0.78 V and −0.57 V (vs SCE), respectively (Fig. 6-d-e). Based on the equation that $E_{NHE} = E_{SCE} + 0.24$ V, the E_{fb} of ZnCr-LDH and $BiVO_4$ are −0.54 and −0.33 V (vs NHE), respectively. For the intrinsic nature of *n*-type semiconductors, the deviation between E_{fb} and the conduction band (CB) is approximately 0.1 V. Thus, the CB potential of ZnCr-LDH and $BiVO_4$ should be −0.64 V and −0.43 V (vs NHE), respectively. Based on the band gap equation of $E_{VB} = -Eg - E_{CB}$, the valence band (VB) potential of ZnCr-LDH and $BiVO_4$ are calculated as 1.86 V and 1.98 V (vs NHE), respectively. Since the CB and VB potentials of ZnCr-LDH are more negative than those of $BiVO_4$, the photogenerated carriers transfer to the opposite direction at the interface of $BiVO_4$/ZnCr-LDH heterojunction, which will form a type II heterojunction. Therefore, the type II heterostructure of ZnCr-LDH and $BiVO_4$ would be possible to promote the separation of photoexcited charges and then maximize the photocatalytic removal efficiency for TC.

The PL measurement of semiconductors was adopted to shed light on the separation and migration ability of the photoinduced carriers. Generally, the higher PL intensity corresponds to higher recombination rate of carriers (Yang et al., 2022b). In Fig. 7a, the fluorescence peak intensity of B-ZCL heterojunction presents much lower than that of ZnCr-LDH and $BiVO_4$, demonstrating the formation of a 3D hierarchical heterostructure through in-situ growth of ZnCr-LDH loaded on $BiVO_4$ can significantly delay the recombination of carriers and improve the utilization of carriers. Among them, 0.5-B-ZCL shows the lowest PL intensity, revealing the lowest recombination probability of photo-induced carriers, consistent with the results of the photodegradation experiment. This could be attributed to the formation of the type-II junction, which could suppress the recombination of photoinduced carriers, with a higher activity than the individual components. In addition to the PL measurement, the photoelectrochemical experiments were further tested to investigate the mobility and separation of photoexcited carriers, as well (Sun et al., 2019). In Fig. 7b, when illuminated by visible light, ZnCr-LDH and $BiVO_4$

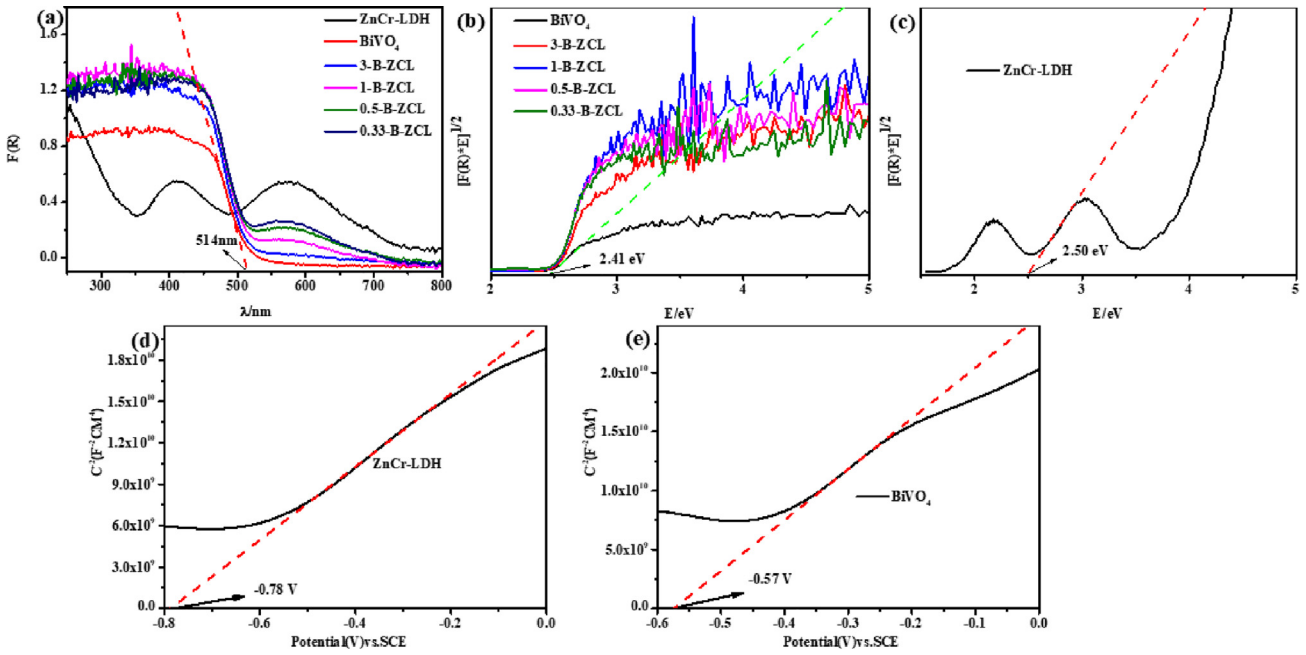

Fig. 6 UV–vis diffuse reflection spectra (a), plots of $(F(R)*E)^{1/2}$ vs energy (hv) of ZnCr-LDH, $BiVO_4$ and a series of B-ZCL heterojunctions (b-c); Mott–Schottky plot of ZnCr-LDH and $BiVO_4$ (d-e).

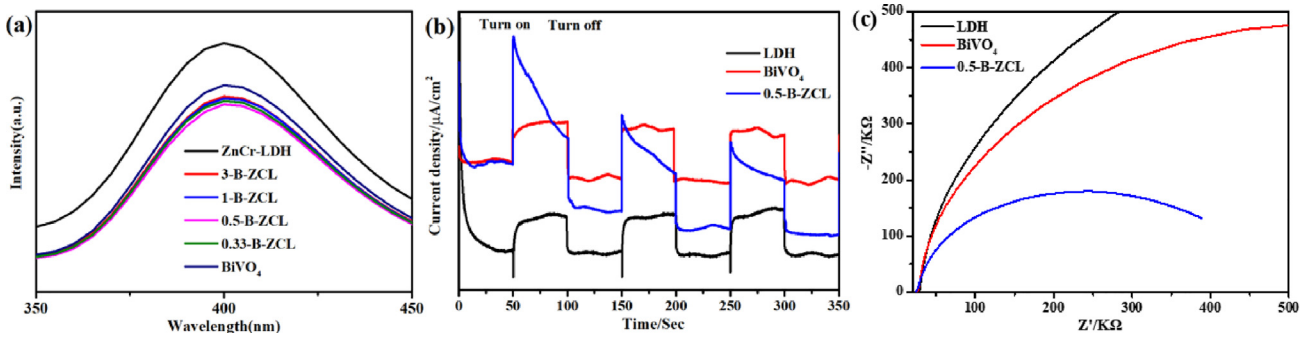

Fig. 7 PL spectroscopy (a), the transient photocurrent response under visible-light irradiation (b) and EIS (c) of ZnCr-LDH, $BiVO_4$ and a series of B-ZCL heterojunctions.

photoelectrodes only generate a weak photocurrent caused by the fast recombination of carriers. Due to the faster separation and migration efficiency of carriers, the photocurrent density of the 0.5-B-ZCL type-II heterojunction is higher than that of ZnCr-LDH and $BiVO_4$ over distinctive on–off cycles. Similarly, the EIS Nyquist plot of ZnCr-LDH, $BiVO_4$ and 0.5-B-ZCL type-II heterojunction is also detected to demonstrate the transport and separation of photoexcited carriers (Fig. 7c). Compared to pure ZnCr-LDH and $BiVO_4$, the 0.5-B-ZCL type-II heterojunction has the smallest arc radius, which indicates a lower resistance and higher charge transfer efficiency between 0.5-B-ZCL type-II heterojunction and electrolyte (Yan et al., 2021). The results of photoelectrochemical experiments illustrate that 3D hierarchical structure combining with 2D/2D interface interactions between ZnCr-LDH and $BiVO_4$ could effectively accelerate the separation of photoinduced charges at the type-II heterojunction interface to enhance the photocatalytic performance.

3.4. Photodegradation mechanism

Combining the above characterization results, the photodegradation mechanism of $BiVO_4$/ZnCr-LDH heterojunction for TC under visible light illumination presented in Fig. 8 is proposed. When irradiated by visible light, electrons in the VB of $BiVO_4$ and ZnCr-LDH are moved to their CB, leaving the corresponding holes in their VB. Simultaneously, driven by the effective interfacial interaction and staggered energy levels, the photo-induced electrons in the CB of ZnCr-LDH flow to the CB of $BiVO_4$, whereas photo-induced holes transfer from $BiVO_4$ to ZnCr-LDH in the opposite direction. Therefore, photo-induced electrons and holes are spatially separated and preserved in $BiVO_4$ and ZnCr-LDH, which can promote the separation efficiency of carriers and prolong their lifetimes of carriers (Li et al., 2019b). Additionally, the electrons accumulated in the CB of $BiVO_4$ can be used as active reducing species, reacting with dissolved oxygen to produce $\bullet O_2^-$ radical.

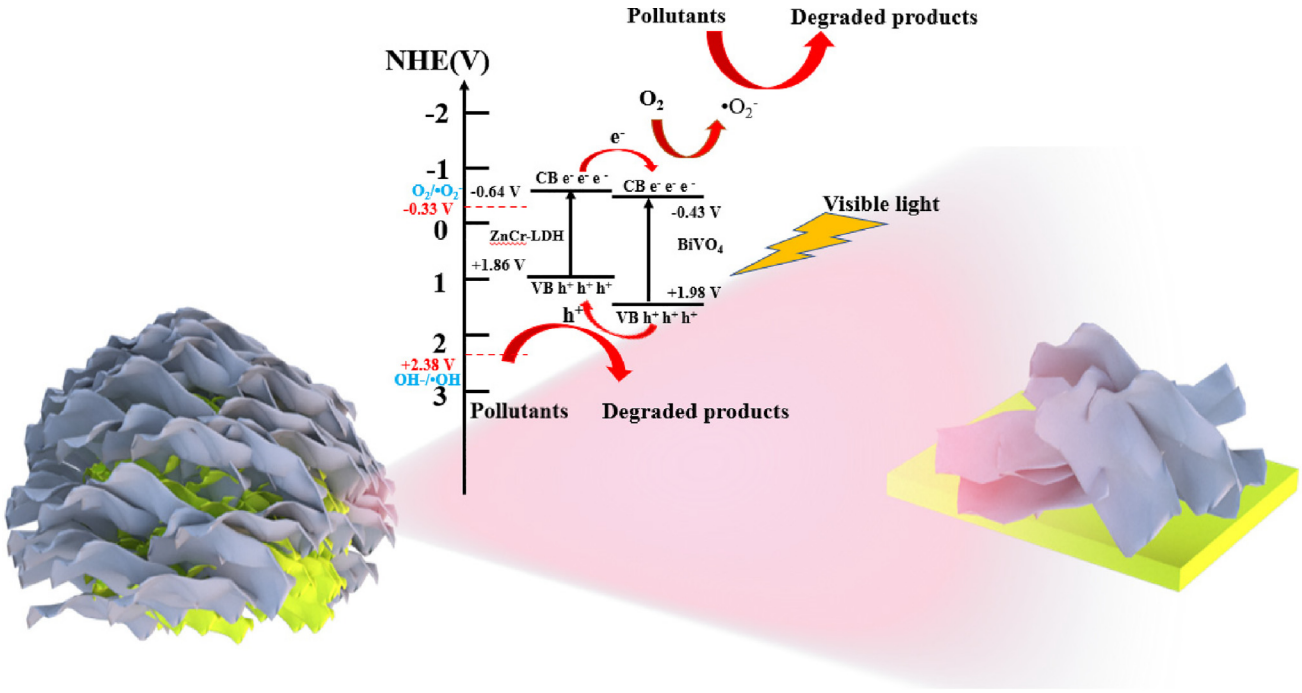

Fig. 8 The proposed photodegradation model over 3D hierarchical $BiVO_4$/ZnCr-LDH type II heterojunction under visible light illumination.

Meanwhile, the h^+ assembled in the VB of ZnCr-LDH could act as oxidizing species to directly participate in the reaction instead of forming •OH radicals, due to the less positive potential of VB. In summary, the notably enhanced photocatalytic degradation activity of 3D hierarchical $BiVO_4$/ZnCr-LDH type-II heterojunction is caused by the following factors: (i) the abundant 2D/2D heterointerfaces between ZnCr-LDH and $BiVO_4$ within 3D hierarchical structure accelerate the transportation and separation of photoexcited carriers; (ii) the 3D hierarchical structure promotes the light absorption, and enables the multiple reflections of incident light; (iii) the enlarged specific surface area provides more active sites to promote the adsorption of reactants to directly participate in the photocatalytic system.

4. Conclusions

In summary, a novel 3D hierarchical $BiVO_4$/ZnCr-LDH type-II heterojunction was successfully prepared, in which 2D ZnCr-LDH nanosheets are in situ attached onto the surface of 2D $BiVO_4$ nanosheets through two-step hydrothermal method. On the one hand, this unique 3D hierarchical structure combining with abundant 2D/2D type-II heterojunction induced by compact heterointerface could promote the separation and migration of photogenerated carriers under visible-light illumination. On the other hand, the 3D hierarchical architecture could enhance the utilization of incident photons through multi-reflection and the higher specific surface area can provide more active sites to accelerate the adsorption of reactants. The photodegradation rate of the optimized 0.5-B-ZCL heterojunction is 3.47 times and 22.43 times higher than that of $BiVO_4$ and ZnCr-LDH for the TC antibiotic. This work reveals that the construction of 3D hierarchical $BiVO_4$/ZnCr-LDH with rich 2D/2D heterostructured interfaces paves the way to improve the photodegradation efficiency for the removal of antibiotic.

Declaration of Competing Interest

The authors declare that they have no known competing financial interests or personal relationships that could have appeared to influence the work reported in this paper.

Acknowledgements

The authors appreciate the financial support of the National Natural Science Foundation of China (No. 21663012), the Natural Science Foundation of Jiangxi province (20181BAB203009), and the Scientific and Technological Project of Education Department of Jiangxi Province (No. GJJ201129 and No. GJJ201132). This work is also partially funded by the Doctoral Start-up Fund (No. 2019BSQD002) and the Project of Jiangxi Science and the Technology Normal University (No. 2020XJYB016), P.R. China.

Appendix A. Supplementary material

Supplementary data to this article can be found online at https://doi.org/10.1016/j.arabjc.2022.104397.

References

Bing, X.M., Li, J., Liu, J., et al, 2018. Biomimetic synthesis of Bi_2O_3/Bi_2WO_6/MgAl-CLDH hybrids from lotus pollen and their enhanced adsorption and photocatalysis performance. J. Photoch. Photobio. A. 364, 449–460.

Cui, Y.W., Ma, J.L., Wu, M.J., et al, 2021. Facet-dependent topo-heterostructure formed by BiOCl and ZnCr-LDH and its enhanced visible-light photocatalytic activity. Sep. Purif. Technol. 254, 117635.

Dong, C.W., Lu, S.Y., Yao, S.Y., et al, 2018. Colloidal synthesis of ultrathin monoclinic $BiVO_4$ nanosheets for Z-scheme overall water splitting under visible light. ACS Catal. 8, 8649–8658.

Fan, H.T., Wu, Z., Liu, K.C., et al, 2022. Fabrication of 3D CuS@$ZnIn_2S_4$ hierarchical nanocages with 2D/2D nanosheet subunits p-n heterojunctions for improved photocatalytic hydrogen evolution. Chem. Eng. J. 433, 134474.

Fu, Y., Ning, F.Y., Xu, S.M., et al, 2016. Terbium doped ZnCr-layered double hydroxides with largely enhanced visible light photocatalytic performance. J. Mater. Chem. A 4, 3907–3913.

Guo, Y., Ao, Y.H., Wang, P.F., et al, 2019. Mediator-free direct dual-Z-scheme Bi_2S_3/$BiVO_4$/$MgIn_2S_4$ composite photocatalysts with enhanced visible-light-driven performance towards carbamazepine degradation. Appl. Catal. B: Environ. 254, 479–490.

Kong, D.Z., Ruan, X.X., Geng, J.K., et al, 2021. 0D/3D $ZnIn_2S_4$/$Ag_6Si_2O_7$ nanocomposite with direct Z-scheme heterojunction for efficient photocatalytic H_2 evolution under visible light. Int. J. Hydrog. Energy 46, 28043–28052.

Lan, M., Fan, G.L., Yang, L., et al, 2014. Significantly enhanced visible-light-induced photocatalytic performance of Hybrid Zn–Cr layered double hydroxide/graphene nanocomposite and the mechanism study. Ind. Eng. Chem. Res. 53, 12943–12952.

Le, S., Li, W., Wang, Y., et al, 2019. Carbon dots sensitized 2D–2D heterojunction of $BiVO_4$/Bi_3TaO_7 for visible light photocatalytic removal towards the broad-spectrum antibiotics. J. Hazard. Mater. 376, 1–11.

Li, C.X., Che, H.N., Liu, C.B., et al, 2019a. Facile fabrication of g-C_3N_4 QDs/$BiVO_4$ Z-scheme heterojunction towards enhancing photodegradation activity under visible light. J. Taiwan Inst. Chem. E. 95, 669–681.

Li, P., Chen, X., He, H., et al, 2018. Polyhedral 30-Faceted $BiVO_4$ microcrystals predominantly enclosed by high-index planes promoting photocatalytic water-splitting activity. Adv. Mater. 30, 1703119.

Li, C., Gu, M., Gao, M., et al, 2022a. N-doping TiO_2 hollow microspheres with abundant oxygen vacancies for highly photocatalytic nitrogen fixation. J. Colloid Interface Sci. 609, 341–352.

Li, J., Li, Y., Zhang, G.K., et al, 2019b. One-Dimensional/Two-Dimensional core–shell-structured Bi_2O_4/BiO_{2-x} heterojunction for highly efficient broad spectrum light-driven photocatalysis: faster interfacial charge transfer and enhanced molecular oxygen activation mechanism. ACS Appl. Mater. Interfaces 11, 7112–7122.

Li, Y.J., Liu, Y.Y., Xing, D.N., et al, 2021b. 2D/2D heterostructure of ultrathin $BiVO_4$/Ti_3C_2 nanosheets for photocatalytic overall Water splitting. Appl. Catal. B: Environ. 285, 119855.

Li, J.Y., Wang, B.W., Pang, Y.Y., et al, 2022b. Fabrication of 0D/1D Bi_2MoO_6/Bi/TiO_2 heterojunction with effective interfaces for boosted visible-light photocatalytic degradation of tetracycline. Colloids Surf. A: Physicochem. Eng. Asp 638, 128297.

Li, L., Yang, Y., Yang, L.Q., et al, 2021a. 3D Hydrangea-like $InVO_4$/$Ti_3C_2T_x$ hierarchical heterosystem collaborating with 2D/2D interface interaction for enhanced photocatalytic CO_2 reduction. ChemNanoMat 7, 815–823.

Li, L., Yang, Y., Zhou, B.Y., et al, 2022c. Dimensional matched ultrathin $BiVO_4$/$Ti_3C_2T_x$ heterosystem for efficient photocatalytic conversion of CO_2 to methanol. Mater. Lett. 306, 130937.

Ling, Y.L., Dai, Y.Z., 2020. Direct Z-scheme hierarchical WO_3/BiOBr with enhanced photocatalytic degradation performance under visible light. Appl. Surf. Sci. 509, 145201.

Liu, J., Li, J., Bing, X.M., et al, 2018. ZnCr-LDH/N-doped graphitic carbon-incorporated g-C_3N_4 2D/2D nanosheet heterojunction with enhanced charge transfer for photocatalysis. Mater. Res. Bull. 102, 379–390.

Liu, Q., Ma, J.F., Wang, K., et al, 2017. BiOCl and TiO_2 deposited on exfoliated ZnCr-LDH to enhance visible-light photocatalytic decolorization of Rhodamine B. Ceram. Int. 43, 5751–5758.

Liu, C., Zhang, X., Li, W., et al, 2020a. Leaf-like $BiVO_4$ nanostructure decorated by nitrogen-doped carbon quantum dots: Binary heterostructure photocatalyst for enhanced photocatalytic performance. Mater. Res. Bull. 122, 110640.

Liu, Y.X., Zheng, Y.T., Xu, Q.C., et al, 2020b. Controllable synthesis of NiSe/$MoSe_2$/MoO_2 3D hierarchical hollow microspheres with enhanced performance for asymmetric supercapacitors. Chem. Eng. J. 387, 124121.

Lu, M.F., Li, Q.Q., Zhang, C.L., et al, 2020. Remarkable photocatalytic activity enhancement of CO_2 conversion over 2D/2D g-C_3N_4/$BiVO_4$ Z-scheme heterojunction promoted by efficient interfacial charge transfer. Carbon 160, 342–352.

Ma, M.Y., Lei, E., Zhao, D., et al, 2022. The p-n heterojunction of $BiVO_4$/Cu_2O was decorated by plasma Ag NPs for efficient photoelectrochemical degradation of Rhodamine B. Colloids Surf. A: Physicochem. Eng. Asp. 633.

Ni, S.N., Zhou, T.T., Zhang, H.N., et al, 2018. BiOI/$BiVO_4$ two-dimensional heteronanostructures for visible-light photocatalytic degradation of Rhodamine B. ACS Appl. Nano Mater. 1, 5128–5141.

Ren, T., Huang, H., Li, N., et al, 2021. 3D hollow MXene@$ZnIn_2S_4$ heterojunction with rich zinc vacancies for highly efficient visible-light photocatalytic reduction. J. Colloid Interface Sci. 598, 398–408.

Sahoo, D.P., Patnaik, S., Rath, D., et al, 2018. Synergistic effects of plasmon induced Ag@Ag_3VO_4/ZnCr LDH ternary heterostructures towards visible light responsive O_2 evolution and phenol oxidation reactions. Inorg. Chem. Front. 5, 879–896.

Sahoo, D.P., Patnaik, S., Parida, K., 2019. Construction of a Z-Scheme dictated WO_{3-X} /Ag/ZnCr LDH synergistically visible light-induced photocatalyst towards tetracycline degradation and H_2 evolution. ACS Omega 4, 14721–14741.

Shen, H.Q., Wang, M., Zhang, X.Z., et al, 2020. 2D/2D/3D architecture Z-scheme system for simultaneous H_2 generation and antibiotic degradation. Fuel 280, 118618.

Shi, Q.R., Zhang, X.Y., Yang, Y., et al, 2021. 3D hierarchical architecture collaborating with 2D/2D interface interaction in NiAl-LDH/Ti_3C_2 nanocomposite for efficient and selective photoconversion of CO_2. J. Energy Chem. 59, 9–18.

Sohail, M., Kim, H., Kim, T.W., 2019. Enhanced photocatalytic performance of a Ti-based metal-organic framework for hydrogen production: Hybridization with ZnCr-LDH nanosheets. Sci. Rep. 9, 7584.

Sun, Z., Li, C., Zhu, S., et al, 2015. Synthesis of $BiVO_4$@C core-shell structure on reduced graphene oxide with enhanced visible-light photocatalytic activity. ChemSusChem 8, 2719–2726.

Sun, Z., Yu, Z., Liu, Y., et al, 2019. Construction of 2D/2D $BiVO_4$/g-C_3N_4 nanosheet heterostructures with improved photocatalytic activity. J. Colloid Interface Sci. 533, 251–258.

Sun, J.C., Zhang, Y.B., Cheng, J., et al, 2014. Synthesis of Ag/AgCl/Zn-Cr LDHs composite with enhanced visible-light photocatalytic performance. J. Mol. Catal. A: Chem. 382, 146–153.

Tan, B., Fang, Y., Chen, Q., et al, 2021. Construction of $Bi_2O_2CO_3$/Ti_3C_2 heterojunctions for enhancing the visible-light photocatalytic activity of tetracycline degradation. J. Colloid Interface Sci. 601, 581–593.

Tang, Z.R., Yu, Q.Q., Xu, Y.J., 2014. Toward improving the photocatalytic activity of $BiVO_4$–graphene 2D–2D composites under visible light by the addition of mediator. RSC Adv. 4, 58448–58452.

Tian, L., Zhao, Y.F., He, S., et al, 2012. Immobilized Cu–Cr layered double hydroxide films with visible-light responsive photocatalysis for organic pollutants. Chem. Eng. J. 184, 261–267.

Wang, C., Ma, B., Xu, S.M., et al, 2017. Visible-light-driven overall water splitting with a largely-enhanced efficiency over a Cu_2O@ZnCr-layered double hydroxide photocatalyst. Nano Energy 32, 463–469.

Wang, S.H., Zhao, L., Gao, L.N., et al, 2022. Fabrication of ternary dual Z-Scheme AgI/$ZnIn_2S_4$ /$BiVO_4$ heterojunction photocatalyst with enhanced photocatalytic degradation of tetracycline under

visible light. Arab. J. Chem. https://doi.org/10.1016/j.arabjc.2022.104159.

Wei, Z., Dai, B.L., Zhu, F.X., et al, 2018. A novel 3D plasmonic p-n heterojunction photocatalyst: Ag nanoparticles on flower-like p-Ag_2S/n-$BiVO_4$ and its excellent photocatalytic reduction and oxidation activities. Appl. Catal. B: Environ. 229, 171–180.

Wu, X.F., Chang, T.L., Fu, Y.X., et al, 2022. Preparation, properties, and photocatalytic mechanism of $In_{2.77}S_4$/$BiVO_4$ heterostructure for tetracycline degradation. J. Mater. Sci: Mater. Electron. 33, 14680–14690.

Xing, Z., Hu, J., Ma, M., et al, 2019. From One to Two. In Situ Construction of an Ultrathin 2D–2D Closely Bonded Heterojunction from a Single-Phase Monolayer Nanosheet. J. Am. Chem. Soc. 141, 19715–19727.

Yan, L.F., Li, W.Y., Zhao, Q.Q., et al, 2021. Enhanced photocatalytic conversion of (3D/2D) $BiVO_4$@Polypyrrole/g-C_3N_4 ternary composites with Z-scheme band alignment for the Antibiotic removal. Colloids Surf. A: Physicochem. Eng. Asp. 624, 126783.

Yang, R.F., Qin, F., Zheng, S.Z., et al, 2022a. Fabrication of full-spectrum response Bi_2O_4/BiO_{2-x} heterojunction as high-performance photocatalyst for organic pollutants removal by a two-step hydrothermal method. J. Mater. Sci. 57, 2467–2482.

Yang, R.F., Qin, F., Zheng, S.Z., et al, 2022b. Fabrication of three-dimensional hierarchical BiOBr/Bi_2O_4 p–n heterojunction with excellent visible light photodegradation performance for 4-chlorophenol. J. Phys. Chem. Solids 161, 110381.

Yang, R.X., Zhu, Z.J., Hu, C.Y., et al, 2020. One-step preparation (3D/2D/2D) $BiVO_4$/$FeVO_4$@rGO heterojunction composite photocatalyst for the removal of tetracycline and hexavalent chromium ions in water. Chem. Eng. J. 390, 124522.

Yao, D., Dong, C., Bing, Q., et al, 2019. Oxygen-Defective ultrathin $BiVO_4$ nanosheets for enhanced gas sensing. ACS Appl. Mater. Interfaces 11, 23495–23502.

Zhao, J.H., Guo, Y., Cai, L.L., et al, 2016. High-performance ultrathin $BiVO_4$ photoanode on textured polydimethylsiloxane substrates for solar water splitting. ACS Energy Lett. 1, 68–75.

Zheng, B.T., Mao, L.H., Shi, J.W., et al, 2021. Facile layer-by-layer self-assembly of 2D perovskite niobate and layered double hydroxide nanosheets for enhanced photocatalytic oxygen generation. Int. J. Hydrog. Energy 46, 34276–34286.

Zhou, W.F., Jiang, T.F., Zhao, Y., et al, 2019. Ultrathin Ti/TiO_2/$BiVO_4$ nanosheet heterojunction arrays for photoelectrochemical water oxidation. J. Alloys Compd. 777, 1152–1158.